ACS APPLIED MATERIALS & INTERFACES

Research Article

www.acsami.org

$TPGS_{2k}$/PLGA Nanoparticles for Overcoming Multidrug Resistance by Interfering Mitochondria of Human Alveolar Adenocarcinoma Cells

Dong-Fang Wang,[†] Wen-Ting Rong,[‡] Yu Lu,[†] Jie Hou,[†] Shan-Shan Qi,[‡] Qing Xiao,[‡] Jue Zhang,[‡] Jin You,[†] Shu-Qin Yu,*[,†,‡] and Qian Xu*[,§,∥]

[†]Jiangsu Key Laboratory for Supramolecular Medicinal Materials and Applications, College of Life Sciences, Nanjing Normal University, Nanjing 210046, People's Republic of China

[‡]Jiangsu Province Key Laboratory for Molecular and Medical Biotechnology, College of Life Sciences, Nanjing Normal University, Nanjing 210046, People's Republic of China

[§]Ministry of Education Key Laboratory of Environmental Medicine and Engineering, School of Public Health, Southeast University, Nanjing 210009, People's Republic of China

[∥]Suzhou Key Laboratory of Environment and Biosafety, Suzhou215123, People's Republic of China

ABSTRACT: In this study, we successfully synthesized D-α-tocopheryl polyethylene glycol 2000 succinate ($TPGS_{2k}$) and prepared $TPGS_{2k}$-modified poly(lactic-*co*-glycolic acid) nanoparticles ($TPGS_{2k}$/PLGA NPs) loaded with 7-ethyl-10-hydroxycamptothecin (SN-38), designated $TPGS_{2k}$/PLGA/SN-38 NPs. Characterization measurements showed that $TPGS_{2k}$/PLGA/SN-38 NPs displayed flat and spheroidal particles with diameters of 80−104 nm. SN-38 was encapsulated in $TPGS_{2k}$ emulsified PLGA NPs with the entrapment efficiency and loading rates of SN-38 83.6 and 7.85%, respectively. SN-38 could release constantly from $TPGS_{2k}$/PLGA/SN-38 NPs in vitro. $TPGS_{2k}$/PLGA/SN-38 NPs induced significantly higher cytotoxicity on A549 cells and the multidrug resistance (MDR) cell line (A549/DDP cells and A549/Taxol cells) compared with free SN-38. Further studies on the mechanism of the NPs in increasing the death of MDR cells showed that following the SN-38 releasing into cytoplasm the remaining $TPGS_{2k}$/PLGA NPs could reverse the P-gp mediated MDR via interfering with the structure and function of mitochondria and rather than directly inhibiting the enzymatic activity of P-gp ATPase. Therefore, $TPGS_{2k}$/PLGA NPs can reduce the generation of ATP and the release of energy for the requisite of P-gp efflux transporters. The results indicated that $TPGS_{2k}$/PLGA NPs could become the nanopharmaceutical materials with the capability to reversal MDR and improve anticancer effects of some chemotherapy drugs as P-gp substrates.

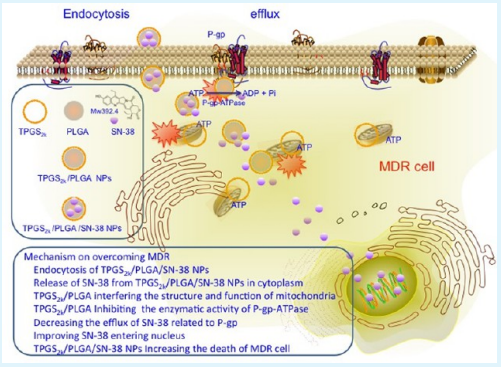

KEYWORDS: *$TPGS_{2k}$, nanopharmaceutical materials, nanoparticles, multidrug resistance, P-glycoprotein, mitochondria, ATP*

INTRODUCTION

Carcinoma cells exposed to one chemotherapy agent may develop multidrug resistance (MDR), the cross-resistance to some chemical constitutions and biological effects unrelated to cytotoxic medicines.[1] MDR is the main obstacle for the anticancer chemotherapy. It is generally recognized that MDR is apparently related to the overexpression of some ATP-binding cassette (ABC) transporters, which consist of P-glycoprotein (P-gp), MDR-related protein (MRP1), and other resistance proteins. As a result, these ABC-transporters can reduce the intracellular concentration of some chemotherapy drugs as the MDR substrates. Among these transporters, the significance of P-gp mediated MDR has been most widely researched. P-gp overexpression is often found in the cancer cells of patients with ineffective chemotherapy. Small molecule P-gp inhibitor, including verapamil, had been applied to codelivery with anticancer drugs to achieve the aim of reversing MDR.[2] Verapamil can make the codelivery drug have a greater anticancer effective or better oral bioavailability.[3] However, the attempt to reverse MDR has not yet obtained promising results because the dose of verapamil as a P-gp inhibitor is significantly greater than the dose of verapamil as an antihypertension drug.[4,5] For fear of these undesirable effects, more considerations have been recently concentrated on some novel delivery materials to modulate P-gp.[6]

Nanopharmaceutical materials (NPMs) applied in nanodrug delivery system (NDDS) should have favorable biocompatible and biodegradable properties. At the same time, NPMs can increase the absorption and the pharmacodynamics of loaded-drug by adjusting the drug release rate and promoting membrane permeability. Recently, the NDDS have raised widespread concern on overcoming MDR.[7−9]

Received: June 26, 2014
Accepted: February 2, 2015
Published: February 2, 2015

DOI: 10.1021/am508340m
ACS Appl. Mater. Interfaces 2015, 7, 3888−3901

These NPMs include D-α-tocopheryl polyethylene glycol 1000 succinate ($TPGS_{1k}$),[10] poly(lactic-*co*-glycolic acid) (PLGA),[11] and so on. $TPGS_{1k}$, a water-solubility vitamin E derivative, is synthesized via trans-esterification of polyethylene glycol 1000 and vitamin E succinate. Mu et al. first proposed $TPGS_{1k}$ as a novel emulsifier in solvent evaporation and extraction preparation for NDDS and proved that $TPGS_{1k}$ could be an effective and safe emulsifier with easy preparation and excellent physicochemical characterization.[12] Liu et al. synthesized a long-chain water-soluble derivative of natural vitamin E, named $TPGS_{2k}$.[13] $TPGS_{2k}$-emulsified PLGA nanoparticles ($TPGS_{2k}$/PLGA NPs) proved preferable merit of the higher cellular uptake over $TPGS_{1k}$-emulsified PLGA nanoparticles ($TPGS_{1k}$/PLGA NPs).[14] $TPGS_{2k}$/PLGA NPs conjugated with folic acid displayed outstanding advantages to cellular uptake and therapeutically effective.[13]

Although $TPGS_{1k}$ or $TPGS_{2k}$ and PLGA as NPMs have been widely used in NDDS,[15] the emphases of investigation still were placed on preparation, physicochemical characteristics, in vitro cytotoxicity, and in vivo biological effects on loaded-drug nanoparticles. It had become clear that $TPGS_{2k}$/PLGA NPs had certain inhibition effect on P-gp. However, the cellular and molecular mechanisms still remain unclear. In our previous research, we demonstrated that $TPGS_{1k}$/PLGA NPs can increase the cellular accumulation of loaded-drug by escaping the recognition of P-gp and affecting efflux microenvironment of MDR cells.[16] The efflux microenvironment is considered to include some subcellular structures and biomolecules that influence the function of P-gp transporter, such as lipid raft in cell membrane,[17] mitochondria,[18] and P-gp Mg^{2+}-ATPase.[19] The effect on the efflux microenvironment could impact the accumulation of chemotherapeutics in organelles. Among NDDS relative to the efflux microenvironment, mitochondrial targeting is a novel strategy for overcoming MDR.[20]

As an active metabolite, 7-ethyl-10-hydroxy-camptothecin (SN-38) is also a topoisomerase 1 inhibitor with anticancer effective 100−1000 times higher than its raw compound, irinotecan.[21] To avoid systemic toxicity of irinotecan in large administrative doses, SN-38 should be administered directly for clinical application to improve anticancer action. Irinotecan or SN-38 is also effective for human small-cell lung cancer independently or in combination with another anticancer drug, such as cisplatin.[22] Owing to the fact that SN-38 is the substrate of P-gp,[23] we chose it as a model drug in the present study.

Nevertheless, there continued to be no evidence to prove the relationship between $TPGS_{2k}$/PLGA NPs and efflux microenvironment. To clarify the mechanisms of $TPGS_{2k}$/PLGA NPs in reversing MDR, we hypothesized that $TPGS_{2k}$/PLGA NPs would change the P-gp efflux microenvironment by means of affecting mitochondrial structure and function (Figure 1C). The aims of this investigation were to assess the effects of $TPGS_{2k}$/PLGA NPs overcoming MDR and its novel cellular and molecular mechanisms. For these objectives, we synthesized $TPGS_{2K}$, prepared $TPGS_{2k}$/PLGA NPs, and delivered anticancer drug SN-38 with the nanoparticles (named $TPGS_{2k}$/PLGA/SN-38 NPs). Then, the effects of $TPGS_{2k}$/PLGA NPs on mitochondria of human alveolar adenocarcinoma cells need to be further evaluated, including the mitochondrial membrane potential, ultramicrostructure, and respiration rate.

EXPERIMENTAL SECTION

Materials. Dichloromethane (DCM), dicyclohexylcarbodiimide (DCC), and 4-dimethylamiopryidine (DMAP) were obtained from Medpep (Shanghai, China). PLGA (lactic acid: glycolic acid = 50:50, viscosity 1.13 dL/g, molecular weight 30 kDa) was ordered from Daigang Biomaterial (Jinan, China). Methoxypolyethylene glycol 2000 ($mPEG_{2k}$), D-α-tocopheryl succinate (α-TOS) and rhodamine-123 (R123) were acquired from Sigma-Aldrich. Cisplatin (cisdiaminedichloroplatinum, DDP), paclitaxel (Taxol), and SN-38 were obtained from Shanghai Knowshine Pharmachemicals. Sodium azide (NaN_3) was purchased from Beyotime (Nantong, China). Verapamil and Coumarin-6 (C6) were purchased from TCI (Tokyo, Japan).

Synthesis of $TPGS_{2k}$. $TPGS_{2k}$ was synthesized based on previously published literature.[14] Briefly, α-TOS, $mPEG_{2k}$, DCC, and DMAP were dissolved in DCM at a stoichiometric ratio of 1:1:2:0.1. The solution was stirred overnight under nitrogen atmosphere. Then, to eliminate the byproducts of the reaction, we filtered and precipitated the solution with precooled diethyl ether. After the obtained precipitant was washed twice with diethyl ether, it was subsequently dissolved in aqua distillate. The final emulsion was gathered from dialyzing against water and filtering to remove impurities. $TPGS_{2k}$ powder was obtained from the filtrate via freeze-drying (Figure 1A).

Preparation of $TPGS_{2k}$/PLGA NPs, Loaded-Drug NPs, and Intracellular Tracing NPs. $TPGS_{2k}$/PLGA NPs were prepared utilizing oil-in-water (O/W) emulsion solvent evaporation based on our previous report.[16] Briefly, PLGA solution (100 mg in 6 mL acetone) was added dropwise into $TPGS_{2k}$ aqueous solution (0.03%, pH 3.0) and mixed under the homogenizer (IKA, German). After the solution was stirred at 1500−1600 rpm by a magnetic stirrer (IKA, German) for 4 h at 25 °C and organic solvent was eliminated by rotary vacuum evaporation, the mixture was centrifuged at 13 500 rpm for 1 h at 4 °C. Collected $TPGS_{2k}$/PLGA NPs were washed twice in deionized water. Then, the acquired precipitation was freeze-dried using a lyophilizer (FL-60 system, China). The resulting nanoparticles were stored at 4 °C for in-depth research.

Nanoparticle-loaded drugs were prepared using O/W emulsion solvent evaporation, as we reported previously.[16] Briefly, SN-38 solution (10 mg, dissolved with dimethyl sulfoxide) was mixed with PLGA solution. The mixture solution was ultrasonicated for 120 s in an ice−water bath to gain a regular organic phase, which was then unhurriedly injected into a homogeneous liquid of 0.03% $TPGS_{2k}$. The acquired O/W emulsion was mixed at 14 000−15 000 rpm for 5 min with a tissue homogenate machine. After the mixed emulsion was lightly stirred using a magnetic stirring apparatus for 4 h at room temperature, the organic solvent was eliminated with a rotary vacuum evaporation (Shanghai DongXi equipment, China) at 45 °C in a thermostatic water bath. A refrigerated microcentrifuge (Eppendorf 5417R, Germany) was employed to collect the resultant sample at 13500 rpm for 45 min. The precipitation was then triple washed with aqua distillate to eliminate surplus SN-38 and emulsifier. Finally, the suspension was lyophilized to obtain powdery SN-38-loaded nanoparticles ($TPGS_{2k}$/PLGA/SN-38 NPs).

To investigate uptake and efflux mechanisms, we also prepared fluorescent-labeled nanoparticles for tracing their intracellular distribution. They were coumarin-6 labeled nanoparticles ($TPGS_{2k}$/PLGA/C6 NPs) for uptake mechanism research and R123 fluorescent-labeled nanoparticles ($TPGS_{2k}$/PLGA/R123 NPs) for efflux mechanism study. Coumarin-6 or R123 substituted for SN-38 was mixed with the organic phase at 0.05% concentration to form $TPGS_{2k}$/PLGA/C6 NPs or $TPGS_{2k}$/PLGA/R123 NPs, respectively.

Physicochemical Characterization. *Surface Morphology.* The surface morphological characteristics of $TPGS_{2k}$/PLGA NPs and $TPGS_{2k}$/PLGA/SN-38 NPs were examined under a scanning electron microscope (SEM, JEOL JSM-5900, Japan).

Particle Size and Zeta Potential. The size, size distribution, and zeta potential of these nanoparticles were determined with dynamic light scattering (DLS; Malvern Zeta Potential Analyzer, UK). Before measurement, the particles were resuspended into deionized water. All tested nanoparticles were measured in triplicate.

Differential Scanning Calorimetry (DSC). The thermal behavior of $TPGS_{2k}$, PLGA, SN-38, $TPGS_{2k}$/PLGA NPs, and $TPGS_{2k}$/PLGA/SN-38 NPs were examined by DSC analysis (Pyris Diamond, PerkinElmer,

DOI: 10.1021/am508340m
ACS Appl. Mater. Interfaces 2015, 7, 3888−3901

Waltham, MA). The thermal analysis was performed with a heating rate of 10 °C/min from 25 to 300 °C under nitrogen atmosphere.

X-ray Diffractometry (XRD). Crystalline state of $TPGS_{2k}$, PLGA, SN-38, and $TPGS_{2k}$/PLGA NPs were evaluated by XRD (D/max-Rc, Ricoh, Japan) using Cu K radiation with 200 mA and 40 kV at a scanning rate of 2°/min over the range of 3−40°.

Loading Efficiency (LE%) and Encapsulation Efficiency (EE%). LE % and EE% of $TPGS_{2k}$/PLGA/SN-38 NPs were carried out with a ultraviolet spectrophotometer (UV-2450, Shimadzu, Japan) as our reported previously.[16] LE% and EE% of SN-38 were calculated as follows formulas.

$$\text{LE}\ (\%) = \frac{\text{weight of SN-38 calculated}}{\text{the weight of drug-loaded nanoparticles}} \times 100$$

$$\text{EE}\ (\%) = \frac{\text{weight of SN-38 calculated}}{\text{weight of SN-38 added}} \times 100$$

Drug Release in Vitro. SN-38 release profile in vitro from $TPGS_{2k}$/PLGA/SN-38 NPs was researched using classical dialysis bag method. The nanoparticles equivalent to SN-38 were dissolved in PBS (containing 0.1% polysorbate 80, v/v) that imitated physiological condition (pH 7.4) and the microenvironment of carcinoma tissue or cancer cells (pH 5.0). After 5 mL of the solution was placed into a dialysis bag (cutoff molecular weight 12 kDa, Millipore), both ends of the bag were solidly fixed with clamps. The bag was slowly shaken (100 rpm) at 37 °C in a thermostatic water bath. Then, 5 mL of the release solution was taken out to detect the concentration of SN-38 using an ultraviolet spectrophotometer at 265 nm. At the same time, an isometric fresh solution was added into the release solution at a designated time interval. The tests were repeated thrice. The accumulated release rate was calculated as follows:

$$\text{drug release rate}\ (\%) = \frac{\text{SN-38 released amount}}{\text{total amount of SN-38 in NPs}} \times 100$$

Biological Effect Research on Human Lung Adenocarcinoma Cells. *Cell Culture.* HFL-I cells (a normal human lung fibroblasts cell line), A549 human lung adenocarcinoma cells and its two types MDR cell lines (A549/DDP cells and A549/Taxol cells; Shanghai Cell Bank, Chinese Academy of Sciences) were used for biological effect research. These cells were cultured in Dulbecco's modified Eagle's medium (DMEM; Life Technologies, Carlsbad, CA) supplemented with 10% HyClone FBS (Thermo Scientific, Waltham, MA) under a humidified atmosphere containing 5% CO_2 in a CO_2 incubator (8000 WJ, Thermo Scientific, Waltham, MA). To retain MDR, A549/DDP cells or A549/Taxol cells were maintained with DDP (2 μg/mL) and Taxol (200 ng/mL), respectively, for 48 h and were further cultured with DDP-free DMEM or Taxol-free DMEM for 48 h before starting the following experiments.

Cell Viability in Vitro. The cell viability of $TPGS_{2k}$ and $TPGS_{2k}$/PLGA NPs on HFL-I cells, a normal human embryonic lung fibroblast, and other cancer cell lines (A549 cells, A549/DDP cells and A549/Taxol cells) were studied in order to detect the cytotoxicity of NPMs. The tests of NPMs were designed at different concentrations (0.125, 0.25, 0.5, and 1.0 mg/mL) and times (24, 48, and 72 h), respectively. The cytotoxicity of $TPGS_{2k}$/PLGA/SN-38 NPs and free SN-38 was studied on A549 cells, A549/DDP cells and A549/Taxol cells for comparing the biological effect of two drug formulations at different concentrations (12.5, 25, 50, and 100 nM, final concentration of SN-38) or time intervals (24, 48, and 72 h). These cells were digested by trypsin for 5 min, harvested, and resuspended in DMEM. The cells were seeded in 96-well plates (Corning, Inc., Corning, NY) at a density of 5×10^4 cells/mL. After these cells grew and were allowed to attach to the well walls until a confluence of 70%, the medium was replaced by 100 μL of FBS-free medium containing above-mentioned tested materials at ranging concentrations and times. The blank medium was used as a control. After treated cells were incubated for 3 h in a CO_2 incubator, WST-1 reagent was used for the quantification of cellular viability based operating manual. The cell percentage viability was calculated as follows:

$$\text{cell viability}\ (\%) = \frac{OD_{\text{test}}}{OD_{\text{control}}}$$

All tests were repeated in triplicate. The viability was expressed as means ± standard deviation from the triplicate experiments.

Cell Apoptosis. The apoptotic effects of $TPGS_{2k}$/PLGA NPs on A549 cells and A549/DDP cells were determined used Annexin V-FITC Apoptosis Detection Kit (Abcam, San Francisco, CA). Tested cells were seeded in 6-well plates (Corning, Inc., Corning, NY) and cultured for 24 h to allow the cells to grow to wall adhesion. After being treated with $TPGS_{2k}$/PLGA NPs at concentrations of 0.25, 0.50, and 1.0 mg/mL for 12 h, the cells were digested with 0.25% trypsin and washed with PBS. The following procedure was completed according to the operating manual.

Intracellular Accumulation Related to Uptake. A549/DDP cell line was incubated in medium containing $TPGS_{2k}$/PLGA/C6 NPs and free coumarin-6, respectively, for 0.25, 0.5, 1, and 2 h. After the medium was replaced, the cells were cultured sequentially with DMEM for 1 h. The quantity of intracellular coumarin-6 was observed under confocal laser scanning microscope (CLSM, Olympus Flowview FV1000, Japan).

Intracellular Accumulation Related to Efflux Pump. A549/DDP cells (1×10^6 cells/mL) were incubated with DMEM (blank control), medium containing verapamil (positive control, 50 μM), and $TPGS_{2k}$/PLGA NPs for 1 h, respectively. Then, after treating with DMEM containing free R123 or $TPGS_{2k}$/PLGA/R123 NPs for 2 h, A549/DDP cells were washed two times with ice−PBS to remove the superfluous R123 or $TPGS_{2k}$/PLGA/R123 NPs. Finally, the cells were incubated with fresh medium for 1 h to allow the efflux of intracellular R123, and the fluorescence of these cells was observed under CLSM.

The mean fluorescence intensity (MFI) standing for the intracellular accumulation of coumarin-6 or R123 was calculated on the fluorescence photographs using ImageJ software.[24]

Cell Mechanization Study. *Mitochondrial Membrane Potential (MMP, $\Delta\Psi_m$).* MMP was assessed using JC-1 mitochondrial membrane potential assay kit (Cayman Chemical, Ann Arbor, MI) under CLSM. A549/DDP cells were seeded in 6-well plates (5×10^5 cells/mL). After reaching a confluence of 80%, these cells were treated in DMEM (blank control), $TPGS_{2k}$/PLGA NPs (0.25 and 0.5 mg/mL) and NaN_3 (10 mM, positive control) for 1 or 4 h, respectively. We followed the operational process based on the manufacturer's protocol. The red-to-green fluorescence ratio (R/G value) was calculated with ImageJ software. The relation between ΔΨm and the R/G value was expressed by the following formula:[25]

$$\Delta\psi_{\text{m}}\ (\%) = \left[1 - \frac{\text{R/G value}_{\text{treatment}}}{\text{R/G value}_{\text{control}}}\right] \times 100$$

Analysis of Respiration Rate. The cellular respiration rate was measured with XF96 cell mito-stress test kit (Seahorse Bioscience, Billerica, MA).[26,27] First, we performed a preliminary test to determine the optimal seeding density of tested cells (A549 cells, A549/DDP cells and A549/Taxol cells) and the adequate concentrations of all tested compounds for the corresponding cell line. The three tested cell lines (3.5×10^5 cells/mL) were seeded on 96-well plates (Seahorse Bioscience, Billerica, MA). In the concentration-dependent study, the cells were treated in $TPGS_{2k}$/PLGA NPs (0.125, 0.25, 0.5, and 1.0 mg/mL) for 4 h. In the time-dependent study, the cell line was treated with $TPGS_{2k}$/PLGA NPs (0.5 mg/mL) for 1 and 4 h. Then, the cells were cultured with Seahorse assay medium (Seahorse Bioscience, Billerica, MA) in an incubator without CO_2 for 1 h to initiate the succedent experiment. After measuring the basal oxygen consumption rate (OCR), we added the following mitochondrial inhibitors sequentially [0.5 μM oligomycin, 0.3 μM carbonyl cyanide-p-trifluoromethoxyphenylhydrazone (FCCP), the mixture of 0.5 μM antimycin A and 0.5 μM rotenone] to assess the changes of OCR using the XF96 Extracellular Flux Analyzer (Seahorse Bioscience, Billerica, MA).

Mitochondrial Ultrastructure Morphology of A549/DDP Cells. To study the intracellular impact of $TPGS_{2k}$/PLGA NPs, we plated A549/

DOI: 10.1021/am508340m
ACS Appl. Mater. Interfaces 2015, 7, 3888−3901

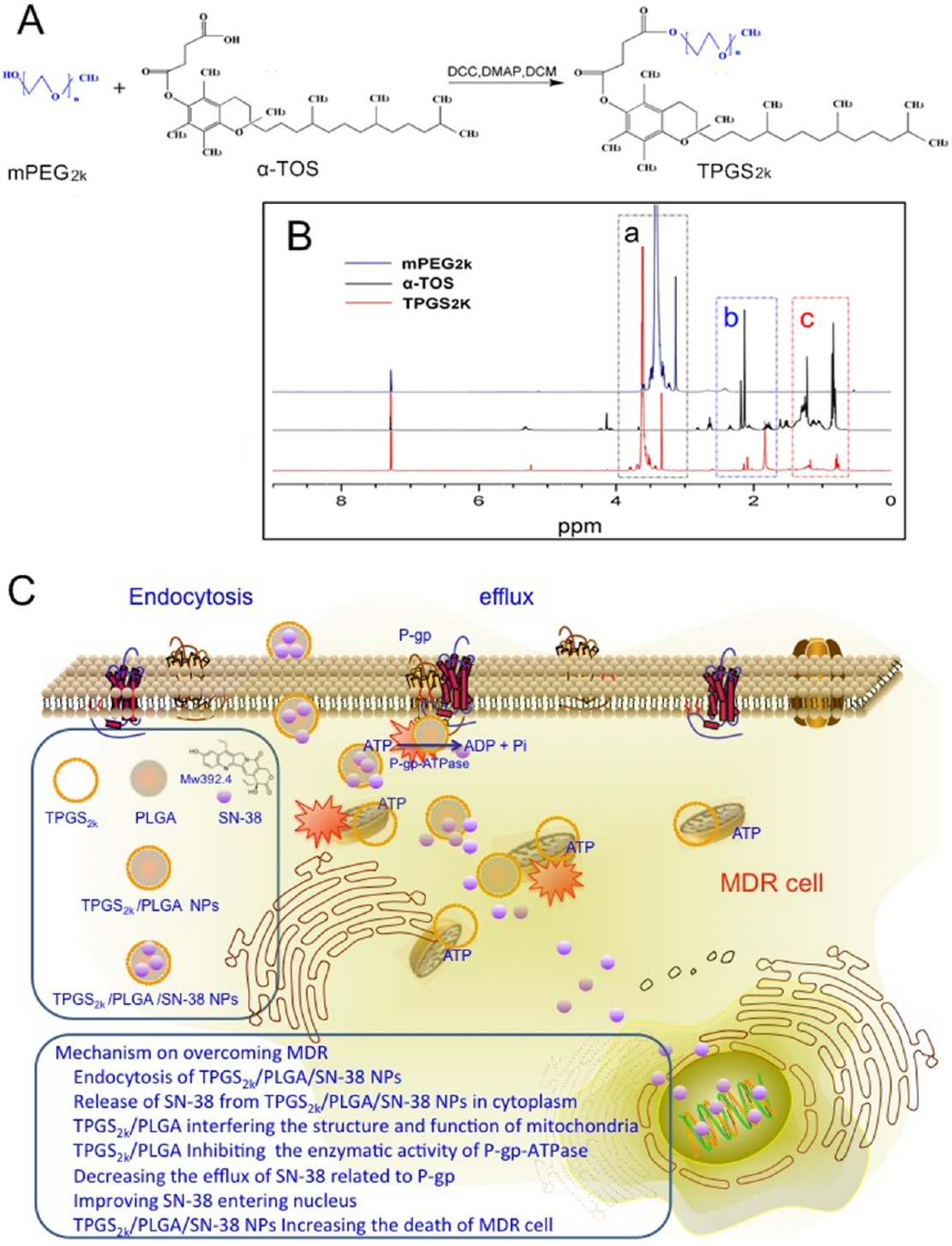

Figure 1. (A) Preparation scheme for $TPGS_{2k}$ polymer. (B) ^1H NMR spectrum of mPEG2k, α-TOS, and $TPGS_{2k}$; the relative shift of the relevant peaks induced by the shielding effect of generated carbonyl are marked as (a) move left, (b) move right, and (c) negligible shift. (C) Schematic illustration of the mechanism on overcoming MDR of $TPGS_{2k}$/PLGA NPs.

DDP cells (3 mL) treated with serum-free medium (as a negative control) or $TPGS_{2k}$/PLGA NPs (0.25, 0.5 mg/mL) in a culture dish. After allowing the cells to culture for 24 h, we digested the cells using trypsin, then harvested the cells and washed them twice with PBS. Following this, the treated samples were fixed using glutaric dialdehyde and osmic acid. The samples were routinely prepared through dehydrating, embedding, cutting ultrathin sections, and collecting on copper grids. Images were viewed under a transmission electron microscope (Hitachi H-7650 TEM, Japan).

ATPase Assay. The affect of $TPGS_{2k}$/PLGA NPs on ATPase activity was measured using P-gp-Glo Assay System (Promega, Madison, WI).[28] Following the kit's instruction, we detected the effects of different tested compounds (TC) on ATPase activity, including sodium orthovanadate (Na_3VO_4, a P-gp ATPase inhibitor), verapamil (a P-gp inhibitor), and $TPGS_{2k}$/PLGA NPs (0.125, 0.25, 0.5, and 1.0 mg/mL). The untreated group (NT) was treated with Pgp-Glo Assay Buffer. The final relative light unit (RLU) of every group was measured with a microplate reader (SpectraMax M2, Molecular Devices, Sunnyvale, CA). If ΔRLU_{TC} (RLU_{Na3VO4} minus

DOI: 10.1021/am508340m
ACS Appl. Mater. Interfaces 2015, 7, 3888−3901

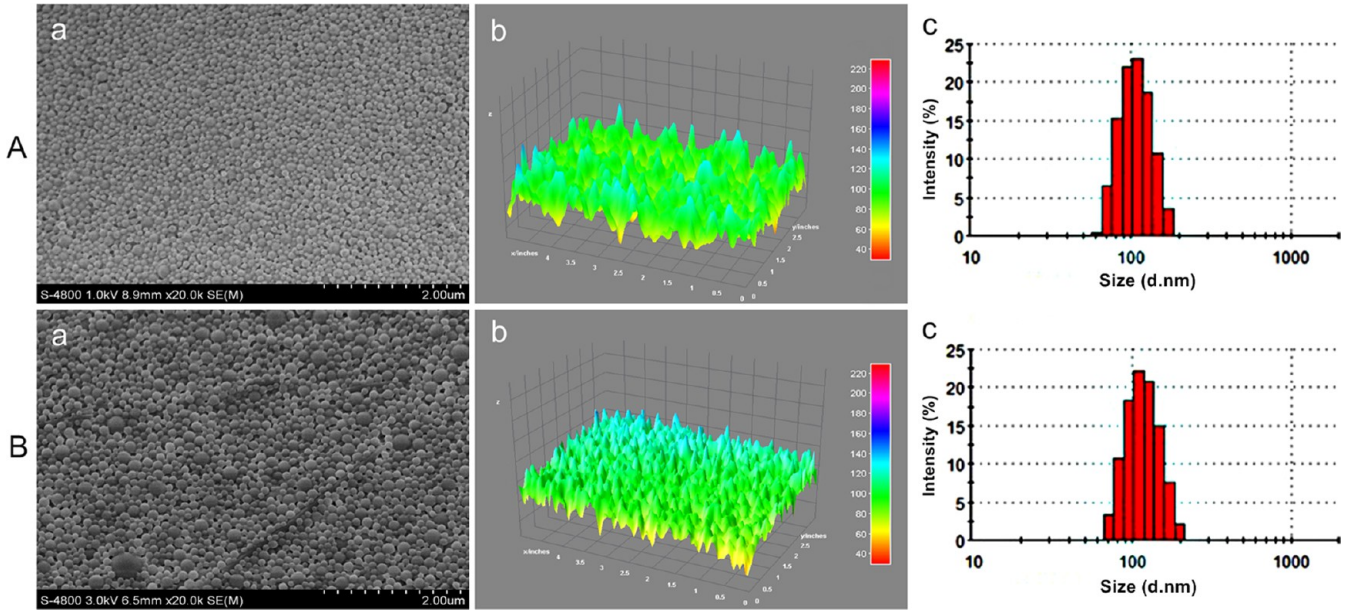

Figure 2. (A) $TPGS_{2k}$/PLGA NPs and (B) $TPGS_{2k}$/PLGA/SN-38 NPs (a) SEM images, (b) size distributions of 3D colored model processed by ImageJ, and (c) size distributions from DLS.

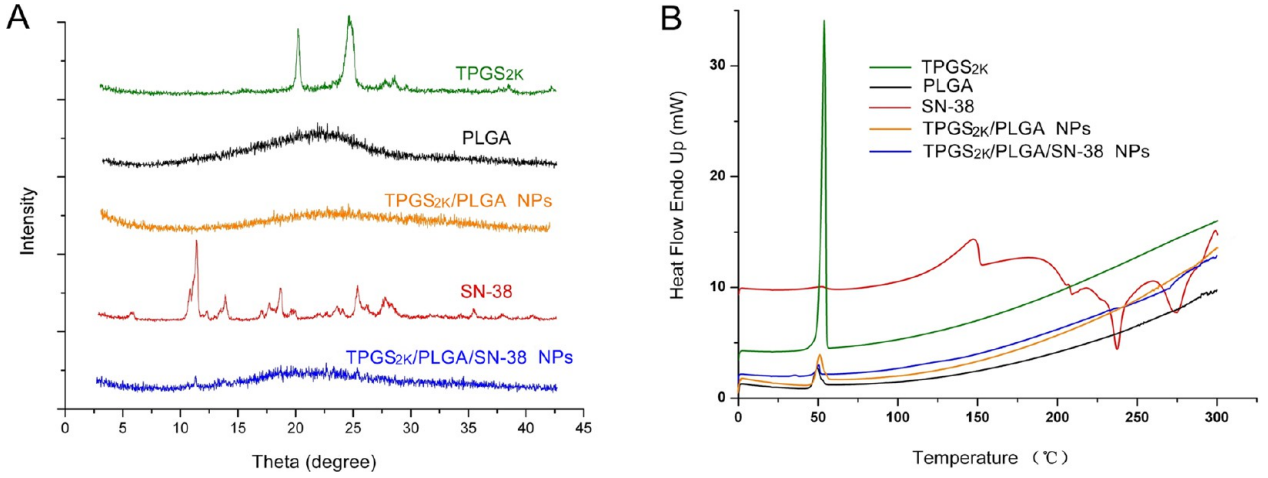

Figure 3. (A) XRD patterns and (B) DSC curves of (green) $TPGS_{2k}$, (black) PLGA, (red) SN-38, (gold) $TPGS_{2k}$/PLGA NPs, and (blue) $TPGS_{2k}$/PLGA/SN-38 NPs.

RLU_{TC}) > ΔRLU_{basal} (RLU_{Na3VO4} minus RLU_{NT}), the tested compound was a P-gp ATPase stimulator; otherwise, it was a P-gp ATPase inhibitor.

Statistical Analysis. Data are expressed as means ± SD. The results were analyzed using differences among the means of groups with an unpaired and two-sided Student's *t*-test. The difference was confirmed significant at $P < 0.05$ and very significant at $P < 0.01$.

RESULTS AND DISCUSSION

Synthesized and Structural Confirmation of $TPGS_{2k}$. In the study, we have successfully synthesized $TPGS_{2k}$ and confirmed its composition by ^1H NMR spectra. Figure 1B shows a comparison of typical ^1H NMR spectra of $mPEG_{2k}$, α-TOS and $TPGS_{2k}$. The generated carbonyl from esterification between $mPEG_{2k}$ and α-TOS enhanced local electronegativity and reduced the shielding effect, which brought about the augment of δ. First, ^1H NMR shows the characteristic peaks of methoxy groups and methylenes of $mPEG_{2k}$ (δ 3.14 and δ 3.40). Due to the decrease of shielding effect, the relevant peaks move left slightly (δ 3.35 and δ 3.66) in ^1H NMR spectra of $TPGS_{2k}$ (Figure 1Ba). On the contrary, the decrease of shielding effect lead to the diminution of δ of methyls (δ 2.12) connecting to the benzene and methylenes (δ 2.17) close to generated carbonyl, which are 2.14 and 2.19 in α-TOS (Figure 1Bb). Finally, the methyls and methylenes far away from the generated carbonyl are scarcely influenced, which means the peaks were obtained with negligible shift (Figure 1Bc). These results demonstrated the similarity and the change of chemical microenvironment between the structures of reactants and products, which suggested that $TPGS_{2k}$ has been successfully synthesized.

Physicochemical Characterization of the Nanoparticles. The diameter and size distribution of nanoparticles play a major effect on drug release behavior and cellular phagocytosis. According to SEM and the 3D models processed by ImageJ,[24] $TPGS_{2k}$/PLGA NPs (Figure 2Aa,b) or $TPGS_{2k}$/PLGA/SN-38 NPs (Figure 2Ba,b) had the global particles with smooth surface and an average diameter about 80 or 90 nm.

DOI: 10.1021/am508340m
ACS Appl. Mater. Interfaces 2015, 7, 3888−3901

The results of DLS (Figure 2Ac,Bc) also confirmed mean diameter of $TPGS_{2k}$/PLGA NPs, which was 104.1 nm, smaller than 109.8 nm of $TPGS_{2k}$/PLGA/SN-38 NPs. Their size distributions displayed a cramped feature (50−110 nm under SEM and 50−120 nm by DLS). The polydispersity index (PDI) of $TPGS_{2k}$/PLGA NPs was 0.037, which was slightly less than that of $TPGS_{2k}$/PLGA/SN-38 NPs (0.05). Both zeta potentials obtained from $TPGS_{2k}$/PLGA NPs and $TPGS_{2k}$/PLGA/SN-38 NPs were negatively charged (−33.78 and −31.23 mV).[13] The results suggested that $TPGS_{2k}$/PLGA NPs or $TPGS_{2k}$/PLGA/SN-38 NPs were dispersed and steadfast.

XRD was employed to settle the existing condition of NPMs and model drug in the NPs. Figure 3A shows the XRD prototype of $TPGS_{2k}$, PLGA, SN-38, $TPGS_{2k}$/PLGA NPs, and $TPGS_{2k}$/PLGA/SN-38 NPs. The characteristic peak (2θ = 21.5 and 25.12°) of $TPGS_{2k}$ in both of nanoparticles disappeared, suggesting that $TPGS_{2k}$ was amorphously distributed on the surface of nanoparticles. At the same time, the decrease or even disappearance of the characteristic peaks of SN-38 (2θ = 10.94, 18.60, and 26.24°) meant that drug had been loaded into these nanoparticles.

Figure 3B presents the DSC curves of NPMs and preparative nanoparticles. For raw materials, the melting endothermic peak (T_m) of SN-38 is at 274.24 °C;[16] there was a small peak at 49.83 °C from the curve of PLGA; and T_m of $TPGS_{2k}$ was 53.81 °C according our detection. Nevertheless, T_m of SN-38 disappeared in $TPGS_{2k}$/PLGA/SN-38 NPs. This result noted that SN-38 in $TPGS_{2k}$/PLGA/SN-38 NPs had been as a noncrystalline form. At the same time, there was no obvious peak to be seen at 45−55 °C based on the curve of $TPGS_{2k}$/PLGA NPs and $TPGS_{2k}$/PLGA/SN-38 NPs. The result indicated that $TPGS_{2k}$ scarcely affected thermogram property of these NPs and $TPGS_{2k}$/PLGA/SN-38 NPs were successfully prepared.

The EE% and LE% of SN-38 in $TPGS_{2k}$/PLGA/SN-38 NPs were 83.6 and 7.85%, respectively. The results indicated that $TPGS_{2k}$/PLGA/SN-38 NPs possessed accredited efficiency of drug loading and encapsulation.

Drug release profiles from $TPGS_{2k}$/PLGA/SN-38 NPs in different pH environments in vitro are presented in Figure 4.

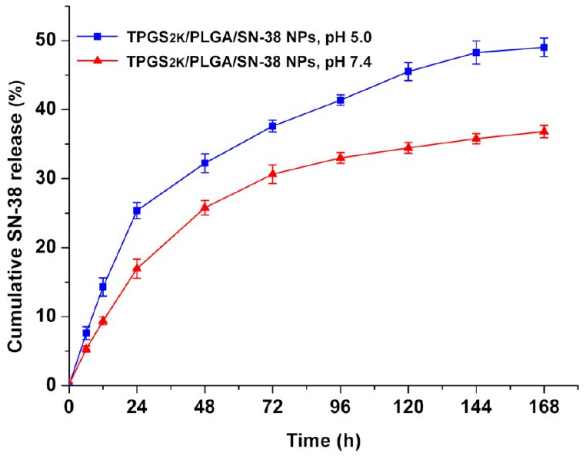

Figure 4. In vitro pH-related release profiles of SN-38 from $TPGS_{2k}$/PLGA/SN-38 NPs in two kinds of PBS (pH 5.0, the intracellular environment of cancer cells, and pH 7.4, the physiological environment). Data represent mean ± SD (n = 3).

The pH values of PBS were 5.0 and 7.4 as the released solution simulated the tumor microenvironment and physiological condition, respectively. An initial burst of SN-38 could be up to 17.85% in the first 12 h at pH 5.0. In the following 168 h, the cumulative release of SN-38 was sustainably increased to 49.03%. It possessed the ability to sustain treatment for the cancer. Moreover, less than 17.32% of SN-38 released from $TPGS_{2k}$/PLGA/SN-38 NPs at 24 h at pH 7.4. The data indicated that $TPGS_{2k}$/PLGA/SN-38 NPs were stable at physiological condition, implying the nanoparticles may have lower toxicity and fewer side effects during anticancer treatment in vivo.

Biological Effects. A549/DDP cells and A549/Taxol cells are human lung adenocarcinoma cell line that are resistant to cisplatin and Taxol, respectively. They also are considered to be an MDR cell line owing to the biological characteristic of P-gp overexpression.[16,29−31] The viability of the tested cell lines incubated with NPMs ($TPGS_{2k}$, $TPGS_{2k}$/PLGA NPs) and model drug (SN-38 or $TPGS_{2k}$/PLGA/SN-38 NPs) with variant concentrations and different times are shown in Figure 5.

Both $TPGS_{2k}$ and $TPGS_{2k}$/PLGA NPs exhibit slight toxicity at higher concentration (Figure 5A) or for a longer incubation time (Figure 5B). For $TPGS_{2k}$/PLGA NPs, when the incubated concentration of $TPGS_{2k}$/PLGA NPs was 0.50 mg/mL, the viability of these cell lines maintained higher levels (82.9 ± 3.27, 83.2 ± 2.37, 83.0 ± 3.27, and 83.9 ± 3.30% in A549, A549/DDP, A549/Taxol and HFL-I cells, respectively) for 24 h. These results showed that the cytotoxicity of $TPGS_{2k}$ and $TPGS_{2k}$/PLGA NPs had no obvious difference on normal cells and cancer cells at tested concentrations. Therefore, 0.50 mg/mL was chosen to explore time-related toxicity and even in-depth study.

After human lung adenocarcinoma cell lines were incubated using free SN-38 for 24 h, obvious cytotoxicity appeared only in the high-concentration groups (50 and 100 nM). The cell viability was 71.7 ± 10.9 and 66.0 ± 3.12% for A549 cells, 74.9 ± 3.58 and 64.5 ± 4.02% for A549/DDP cells, and 75.9 ± 4.25 and 66.0 ± 3.12% for A549/Taxol cells. Instead, when incubated with $TPGS_{2k}$/PLGA/SN-38 NPs the cell viability decreased to 48.1 ± 2.63 and 33.9 ± 6.06% for A549/DDP cells and 55.4 ± 2.77 and 33.9 ± 6.06% for A549/Taxol cells (Figure 5C). After treatment for 48 and 72 h, the cell viability treated with $TPGS_{2k}$/PLGA/SN-38 NPs achieved more obvious decrease compared to free SN-38 (Figure 5D). In fact, $TPGS_{2k}$/PLGA/SN-38 NPs achieved higher cellular mortality at each concentration and incubation times than free SN-38.

To verify the influence of these nanoparticles on human lung adenocarcinoma cells apoptosis, we performed the Annexin V-FITC/PI apoptosis assay of A549 cells and A549/DDP cells to distinguish apoptosis cells from normal cells. The effects of $TPGS_{2k}$/PLGA NPs on apoptosis and necrosis of A549 cells and A549/DDP cells were quantified by total percentage of early apoptosis (Q3) and late apoptosis (Q2). As shown in Figure 6, compared to the apoptosis percentages of the blank control (4.06% for A549 cells and 3.59% for A549/DDP cells), after incubation with $TPGS_{2k}$/PLGA NPs (0.25, 0.50, and 1.0 mg/mL) for 12 h, the induced apoptosis percentages were increased to 7.47, 18.2 ($p < 0.05$), and 31.6% ($p < 0.01$) in A549 cells, to 6.26, 11.0, and 31.2% ($p < 0.01$) in A549/DDP cells. The results were consistent with the viability detection experiments and further revealed that the tested cell viability

DOI: 10.1021/am508340m
ACS Appl. Mater. Interfaces 2015, 7, 3888−3901

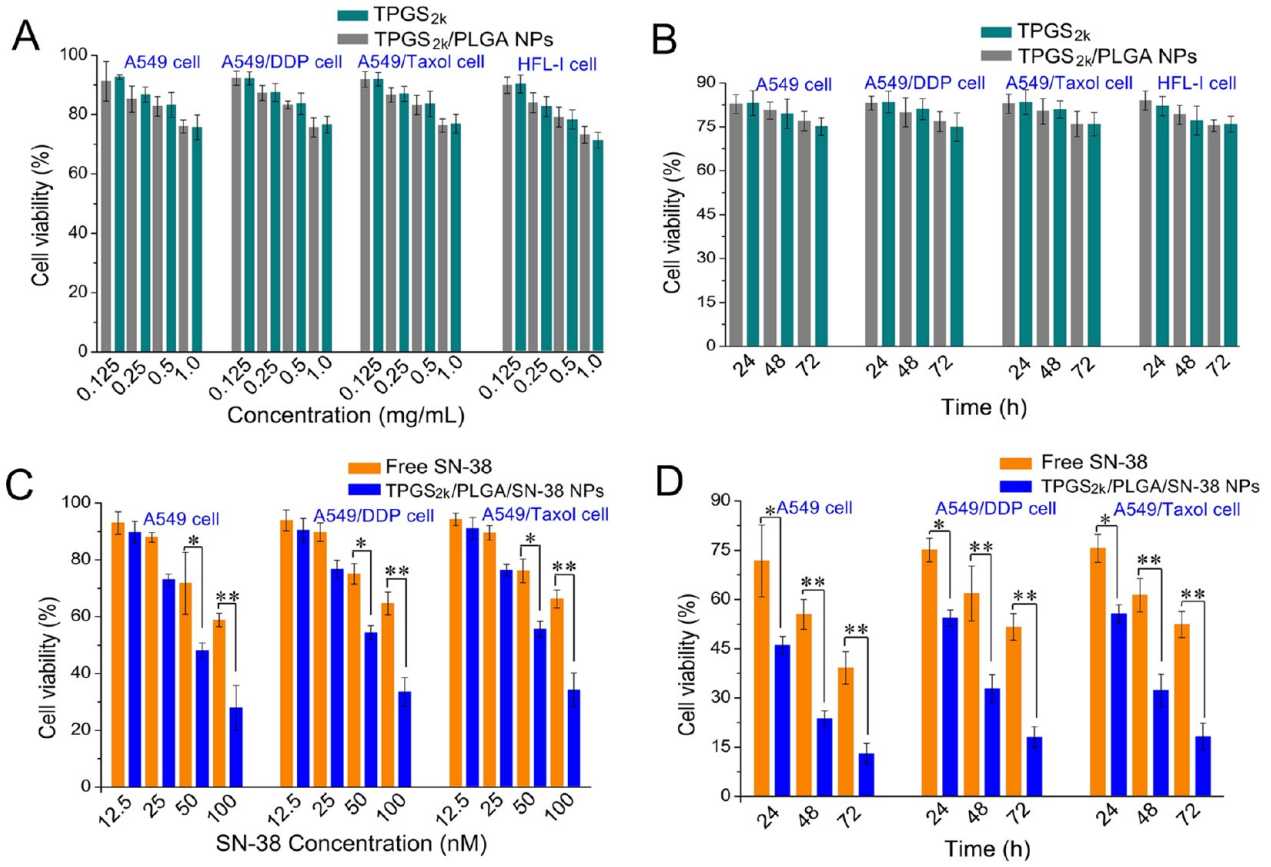

Figure 5. Viability of cancer cells and normal cells was determined using WST-1 assay. A549 cells, A549/DDP cells, A549/Taxol cells, and HFL-I cells were incubated with $TPGS_{2k}$ and $TPGS_{2k}$/PLGA NPs (A) at different concentrations and (B) for different times. A549 cells, A549/DDP cells, and A549/Taxol cells were incubated with free SN-38 and $TPGS_{2k}$/PLGA/SN-38 NPs (C) of different concentrations and (D) for different times. The results are expressed as viability (%) relative to control group. Data represent mean ± SD (n = 3).

decreased after the cells were treated with $TPGS_{2k}$/PLGA NPs, mainly owing to cells apoptosis.

Transmission electron microscopy (TEM)[32] and fluorescent tracing method can be applied to the conformation of endocytosis process of the nanoparticles. Certainly, TEM is a better method for the uptake of nanoparticles. Then, coumarin-6-labeled NPs ($TPGS_{2k}$/PLGA/C6 NPs) were used for uptake research on account of their lower leakage rate and higher fluorescent capacity.[33] Owing to R123 being a P-gp substrate and an acknowledged fluorescent tracer, we used R123 fluorescent-labeled NPs ($TPGS_{2k}$/PLGA/R123 NPs) for efflux mechanism study.[34,35] Figure 7A presents the intracellular distribution of coumarin-6 in A549/DDP cells incubated by coumarin-6 or $TPGS_{2k}$/PLGA/C6 NPs at four different times (0.25, 0.5, 1, and 2 h). Cellular MFI of coumarin-6 and $TPGS_{2k}$/PLGA/C6 NPs at 0.25 h was 7.90 ± 0.747 and 12.3 ± 1.07%, respectively (Figure 7C). The nanoparticles got a 55.7% fluorescent increase compared with coumarin-6. While the treating time was prolonged, the fluorescent increase rates were 69.5, 126.3 (P < 0.01, compared with coumarin-6), and 141.5% (P < 0.01, compared with coumarin-6) at 0.5, 1, and 2 h, respectively. The results indicated that the MFI increase of coumarin-6 and $TPGS_{2k}$/PLGA/C6 NPs had also certain property of time-dependent intracellular accumulation. Moreover, $TPGS_{2k}$/PLGA/C6 NPs can significantly increase the uptake of coumarin-6 in A549/DDP cells.

Figure 7B shows the microscopic images related to the intracellular accumulation of R123 related to efflux pump. The presence of verapamil significantly enhanced cellular concentration of R123. As expected, intracellular accumulation of R123 was enhanced obviously after A549/DDP cells were pro-cultured with $TPGS_{2k}$/PLGA NPs for 1 h. Similarly, while these cells were treated with $TPGS_{2k}$/PLGA/R123 NPs instead of free R123, the intracellular accumulation of R123 in each group significantly enhanced, respectively, as well. As shown in Figure 7D, $TPGS_{2k}$/PLGA/R123 NPs for 1 h, MFI increased by 60.1% (P < 0.05, vs free R123) in the medium control group. After cells were pro-cultured with $TPGS_{2k}$/PLGA NPs for 1 h, subsequently cultured with $TPGS_{2k}$/PLGA/R123 NPs for 1 h, the increase of MFI had a significant difference (49.1%, P < 0.05) comparing with free R123 group. Similar results can be seen in verapamil group, the increase of MFI was 49.5% (P < 0.05, vs free R123). Therefore, $TPGS_{2k}$/PLGA NPs could overcome MDR by decreasing efflux of P-gp substrates.

These results indicated there was only fainter efflux for R123 after treated with $TPGS_{2k}$/PLGA/R123 NPs in A549/DDP cells. We supposed that $TPGS_{2k}$/PLGA or $TPGS_{2k}$ may inhibit the efflux for P-gp substrate after $TPGS_{2k}$/PLGA NPs released loaded-drug. As a result, $TPGS_{2k}$/PLGA NPs prolonged intracellular residence time and enhanced the therapeutic effect of the anticancer drug by more effective uptake and fainter efflux in MDR cells.

Mechanisms of Overcoming MDR. It was also confirmed that $TPGS_{2k}$/PLGA/SN-38 NPs could enhance the cytotoxicity of SN-38 on A549/DDP cells, which provided a potential design of pharmacological inactive excipients with P-gp

DOI: 10.1021/am508340m
ACS Appl. Mater. Interfaces 2015, 7, 3888−3901

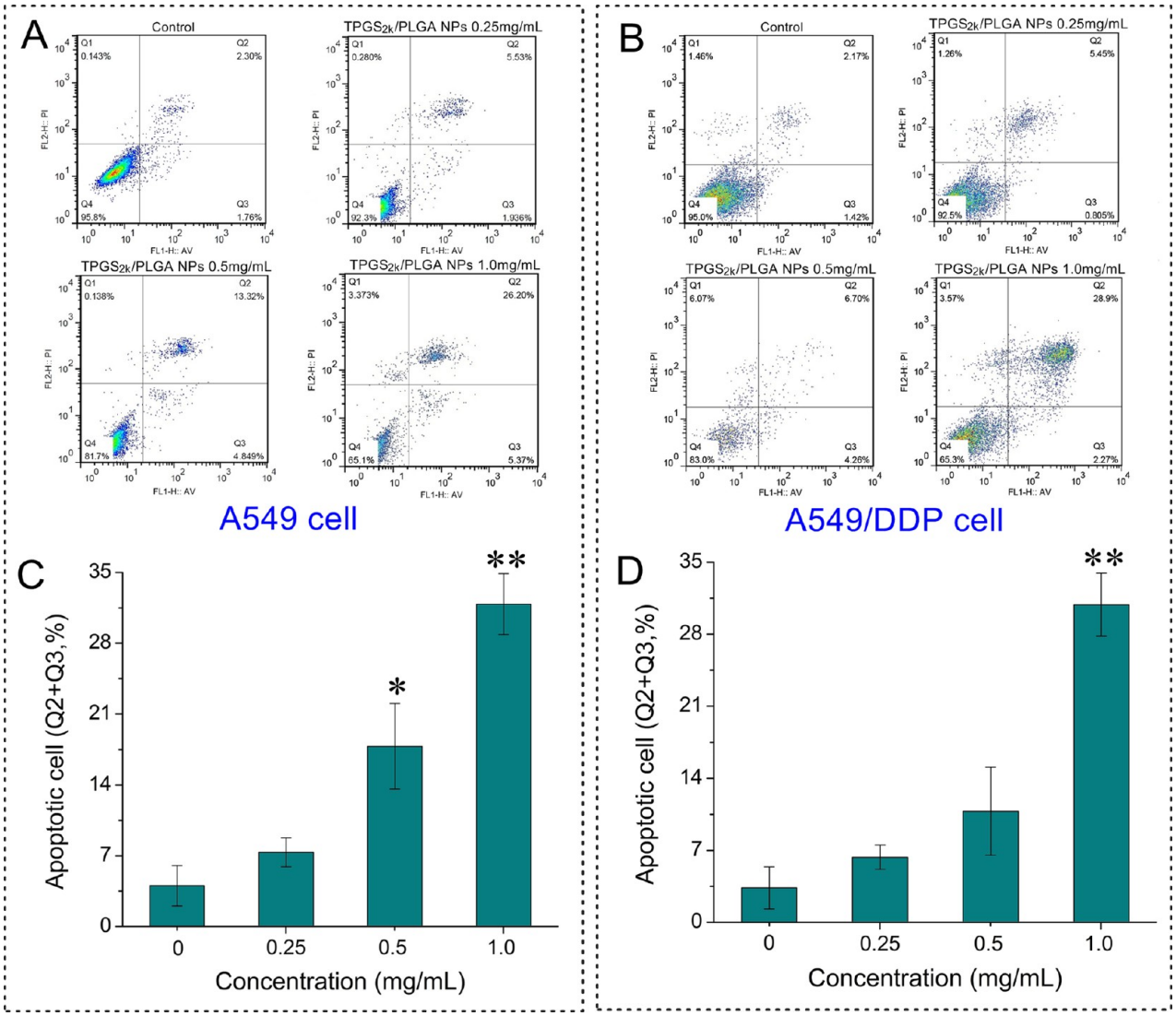

Figure 6. Apoptosis and necrosis of A549 cells and A549/DDP cells treated with $TPGS_{2k}$/PLGA NPs (0.25, 0.5, and 1.0 mg mL^{-1}) for 12 h in vitro. (A and B) Typical four quadrants of FACS analyses in the frames represent (Q1) cells undergoing necrosis, (Q2) late apoptotic cells, (Q3) early apoptotic cells, and (Q4) viable cells. (C) and (D) percentages of apoptosis (Q2 + Q3). Data represent mean ± SD (n = 3). (*) $p < 0.05$ and (**) $p < 0.01$ versus negative control.

modulators. For this reason, we further studied the cellular and molecular mechanisms of $TPGS_{2k}$/PLGA NPs in reversing MDR. As is well-known, inhibition P-gp efflux pump could increase the concentration of P-gp substrate in MDR cells. P-gp belongs to ATP-binding cassette transporters connected with energy-related efflux microenvironment.[36] Hence, we proposed that $TPGS_{2k}$/PLGA NPs acting on P-gp maybe affect the intracellular microenvironment of efflux, especially the structure and function of mitochondria.[37] In this investigation, we concentrated on the influence of $TPGS_{2k}$/PLGA NPs on MMP, ultrastructure, and cellular OCR of mitochondria in A549/DDP cells.

MMP. A normal MMP is required to maintain mitochondrial function, such as oxidative phosphorylation and ATP synthesis. In the present research, JC-1 was introduced fluorescent probe to detect the effect of $TPGS_{2k}$/PLGA NPs on MMP.[25] The green fluorescence intensity in cells can represent the level of MMP. As shown in Figure 8, MMP ($\Delta\Psi_m$) of A549/DDP cells was 5.39% ($p < 0.01$) and 14.3% ($p < 0.01$) in $TPGS_{2k}$/PLGA NPs at concentrations of 0.25 and 0.50 mg/mL, respectively. The results indicated that $TPGS_{2k}$/PLGA NPs caused the change of MMP with concentration-dependent characteristic. Then, after the cells were cultured with $TPGS_{2k}$/PLGA NPs (0.25 and 0.50 mg/mL) for 1 and 4 h, we found that the $\Delta\Psi_m$ was 27.4% ($p < 0.01$) and 35.6% ($p < 0.01$), indicating that $TPGS_{2k}$/PLGA NPs depolarized the MMP in a time-dependent manner. Dong et al. reported that $TPGS_{1k}$ could change the MMP of MDA-MDB-435/LCC6, a P-gp overexpress human melanoma cell.[38] We conjecture that after the drug was released from loaded-drug $TPGS_{2k}$/PLGA NPs in A549/DDP cells, $TPGS_{2k}$ may play an important role on modulating the MMP of MDR cells.

On the other hand, the decrease of MMP was part of the performance of impaired mitochondrial function. Though the disruption of MMP was observed in A549/DDP cells cocultured with $TPGS_{2k}$/PLGA NPs (0.25 and 0.5 mg/mL; Figure 8), there was no obviously apoptosis found at the concentrations (Figure 6). In fact, $TPGS_{2k}$/PLGA NPs rarely induced the apoptosis, even at a higher concentration in A549/DDP cells. Hence, $TPGS_{2k}$/PLGA NPs reverse MDR just by

DOI: 10.1021/am508340m
ACS Appl. Mater. Interfaces 2015, 7, 3888−3901

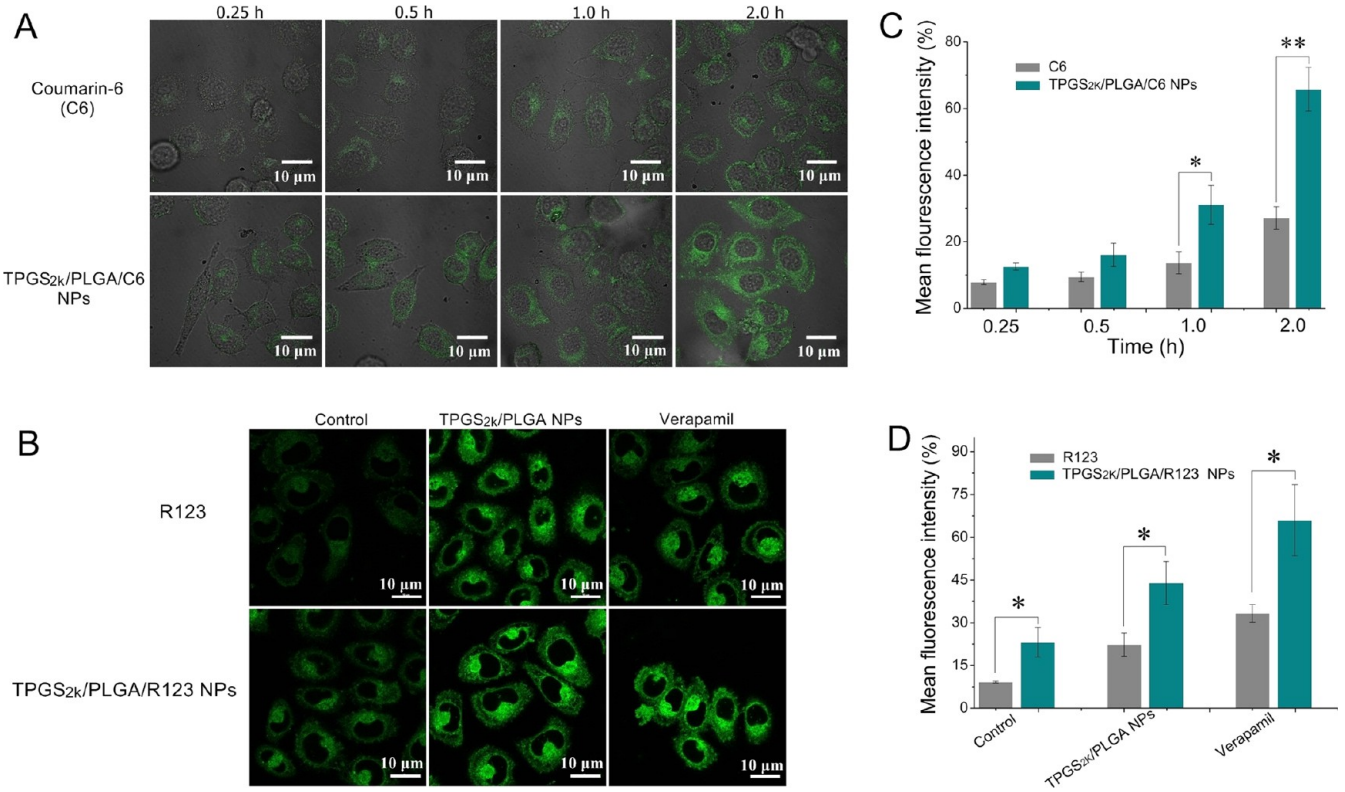

Figure 7. Effects of $TPGS_{2k}$/PLGA NPs on uptake and efflux observed under confocal laser scanning microscopy. (A) Intracellular coumarin-6 accumulation images of A549/DDP cells treated with coumarin- 6 and $TPGS_{2k}$/PLGA/C6 for 0.25, 0.5, 1.0, and 2.0 h. (B) Intracellular R123 accumulation images of A549/DDP cells treated with R123 or $TPGS_{2k}$/PLGA/R123 NPs incubated with the efflux inhibitor verapamil. (C and D) Mean fluorescence intensities (MFIs) calculated by ImageJ. Data represent mean ± SD (n = 3). (*) $P < 0.05$; (**) $P < 0.01$ vs free R123 group. Data represent mean ± SD (n = 3). (*) $P < 0.05$ and (**) $P < 0.01$, compared with free 6-coumarin or R123.

being harmful to the efflux microenvironment and having little affect on cell viability.

Cellular Respiration Rate. To further study the mechanism of $TPGS_{2k}$/PLGA NPs on the mitochondria of the human lung adenocarcinoma cell line, we measured the cellular OCR of mitochondria used XF cell Mito stress test kit. The kit involved the ATP coupler oligomycin, the mitochondrial uncoupler FCCP, and the mitochondrial inhibitors antimycin A and rotenone. They can be used to calculate the spare respiratory capacity of cells and measure the four key parameters of mitochondrial function; they are basal respiration, ATP turnover, proton leak, and maximal respiration.[39,40] Hence, we analyzed the different states of mitochondrial respiration through determination of OCR in A549 cells, A549/DDP cells, and A549/Taxol cells treated with DMEM (negative control group), NaN_3 (positive control group) and $TPGS_{2k}$/PLGA NPs, respectively, in different concentrations (0.125, 0.25, 0.5, and 1.0 mg/mL) or different time points (1 and 4 h). These results are presented in Figure 9.

In concentration-dependent tests, $TPGS_{2k}$/PLGA NPs at every concentration could influence on the basal OCR of A549 (Figure 9A), A549/DDP (Figure 9C), and A549/Taxol cells (Figure 9E). For A549/DDP cells (Figure 9C), the spare respirator capacity was decreased by 6.92, 10.3, 24.7, and 51.7%, respectively, compared with the negative control group after these cells were treated by $TPGS_{2k}$/PLGA NPs at concentrations of 0.125, 0.25, 0.5, and 1.0 mg/mL. The disrupted effect of $TPGS_{2k}$/PLGA NPs on ATP synthesis was relative to blocking the proton channel of the F_0 portion ATP synthase and to uncoupling electron transport. The decreased rates of coupling efficiency were 4.83, 13.9, 21.3, and 40.5%, respectively, at different concentrations. However, the respirator reserve capacity was decreased by 4.97, 14.53, 38.8, and 59.8%, while NPs at tested concentrations were blended with mitochondrial inhibitors rotenone and antimycin A. Analogous disrupted effects of $TPGS_{2k}$/PLGA NPs on cellular respiration rate were also found in A549 cells and A549/Taxol cells (Figure 9A,E). Accordingly, the reduction effects of $TPGS_{2k}$/PLGA NPs on the spare respirator capacity, coupling efficiency, and respirator reserve capacity possessed the characteristic of concentration-dependent.

In time-dependent tests (Figure 9B,D,F), for instance, A549/DDP cells, the spare respirator capacity was decreased by 16.7 and 25.7% compared with the negative group after treated by $TPGS_{2k}$/PLGA NPs (0.5 mg/mL) at different time of 1 and 4 h (Figure 9B). The decrease rates of the coupling efficiency were 16.9% (1 h) and 19.8% (4 h), respectively. The result indicated that $TPGS_{2k}$/PLGA NPs for 4 h had significantly disrupted effect on ATP synthesis. Moreover, $TPGS_{2k}$/PLGA NPs had relative disrupted effect on respirator reserve capacity, which decreased by 18.9 and 29.7% at different time. Similar disrupted effects of $TPGS_{2k}$/PLGA NPs on cellular respiration rate were also noted in A549 cells and A549/Taxol cells (Figure 9D,F). Therefore, the decreasing effects of $TPGS_{2k}$/PLGA NPs on the spare respirator capacity, coupling efficiency, and respirator reserve capacity exhibited the characteristic of time-dependent.

Intracellular biochemical reactions are the process of substrate uptake through a series of enzymatically controlled oxidation and reduction reactions, resulting in the production of ATP.[41] We gain valuable insights into the role of $TPGS_{2k}$/

DOI: 10.1021/am508340m
ACS Appl. Mater. Interfaces 2015, 7, 3888−3901

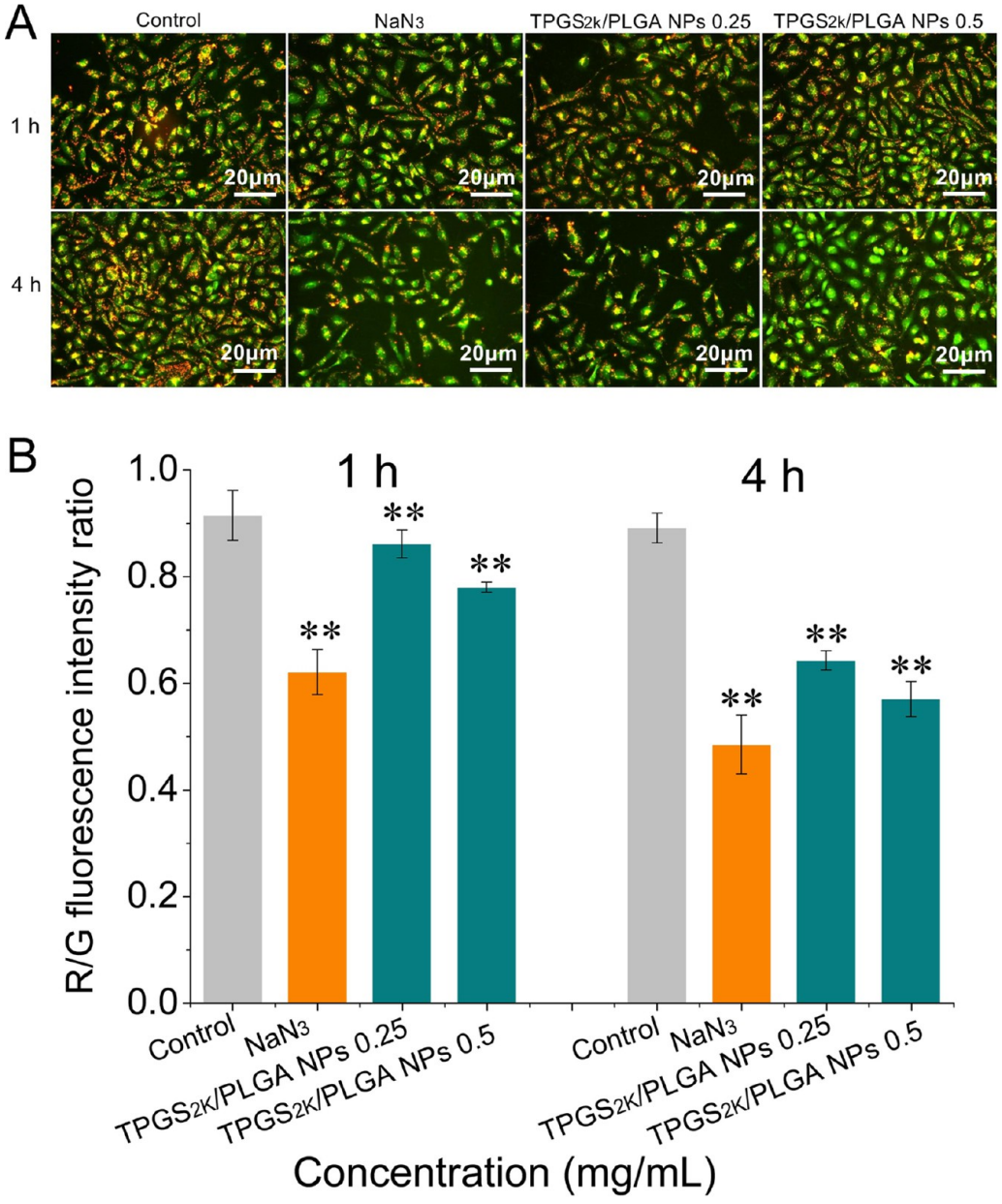

Figure 8. Time- and concentration-dependence effects of $TPGS_{2k}$/PLGA NPs on the MMP in A549/DDP cells using the JC-1 probe method. (A) Representative images of A549/DDP cells under fluorescence microscope incubated for 1 and 4 h with $TPGS_{2k}$/PLGA NPs at 0.25 or 0.5 mg/mL, and NaN_3 as the positive control. (B) The quantitative analysis of fluorescence microscopy images JC-1 red/green fluorescence intensity ratio by ImageJ (mean ± SD, $n = 8$). (*) $p < 0.05$ and (**) $p < 0.01$, compared with negative control at the same time point.

PLGA NPs on mitochondrial respiration function according to OCR in vitro (Figure 9). $TPGS_{2k}$/PLGA NPs reduced cell ATP generation in a concentration-dependent and a time-dependent manner. Recently, we reported that polysorbate 80, a nonionic surfactant and emulsifier employed in the pharmaceutical and food industries could affect the OCR in caco-2 cell.[26] Some inhibitors of complexes I, II, and III in the mitochondrial respiratory chain can be developed as an anticancer drug for targeting mitochondria.[42] Neuzil et al. considered that TPGS could be the inhibitor of complex II.[43] The inhibiting effect was achieved via competitive binding to coenzyme Q sites on account of containing moieties resembles coenzyme Q.[44,45] Our results suggest that $TPGS_{2k}$, a novel derivative of vitamin E, may also be an inhibitor of complex II. This inference needs to be confirmed by further study.

Mitochondrial Ultrastructure Morphology. To further investigate the influence of $TPGS_{2k}$/PLGA NPs on the ultrastructure of mitochondria, we have studied on the morphology of A549/DDP cell under TEM (Figure 10). The A549/DDP cells were treated with serum-free medium (control group) or $TPGS_{2k}$/PLGA NPs (0.25 and 0.50 mg/mL) for 24 h. The mitochondria of A549/DDP cells at the control group (Figure 10A) were complete double membrane structures with an inner membrane and a smooth outer membrane. The polymorphic cristae within the mitochondria matrix were perpendicular to the axis of mitochondria. Moreover, electron density was low and uniformly distributed in the matrix. Mitochondria at $TPGS_{2k}$/PLGA NPs group (Figure 10B,C) were still present oval but with the incrassate cristae. Moreover, the double membrane structure of mitochondria suffered

DOI: 10.1021/am508340m
ACS Appl. Mater. Interfaces 2015, 7, 3888−3901

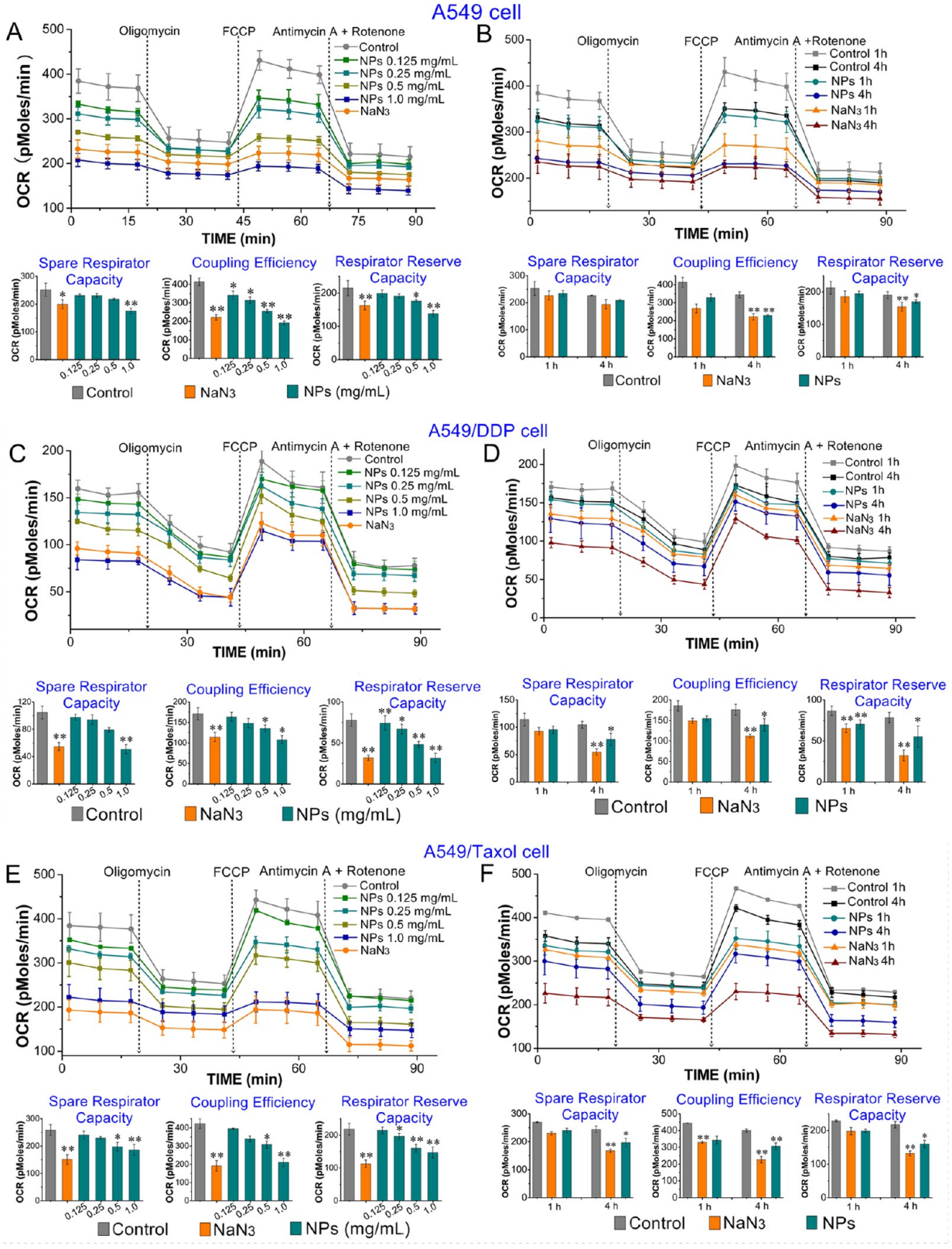

Figure 9. Concentration- and time-dependence effects of $TPGS_{2k}$/PLGA NPs on (A and B) mitochondrial respiration of A549 cell, (C and D) A549/DDP cell, and (E and F) A549/Taxol cell were measured by the Seahorse extracellular flux analyzer. The line graph shows the OCR of tested cells exposed sequentially to the modulator of mitochondrial respiration (oligomycin, FCCP, antimycin A, and rotenone) following treated with $TPGS_{2k}$/PLGA NPs at different concentrations (0.125, 0.25, 0.5, and 1.0 mg/mL) for 4 h, or with $TPGS_{2k}$/PLGA NPs at the same concentration (0.5 mg/mL) for different times (1 or 4 h). FBS-free medium was a negative control, and NaN3 (10 μM) was a positive control. The column diagrams are spare respirator capacity, coupling efficiency and respirator reserve capacity by the mitochondrial OCR data analysis. Data represent mean ± SD (n = 3). (*) $p < 0.05$ and (**) $p < 0.01$ versus negative control.

DOI: 10.1021/am508340m
ACS Appl. Mater. Interfaces 2015, 7, 3888−3901

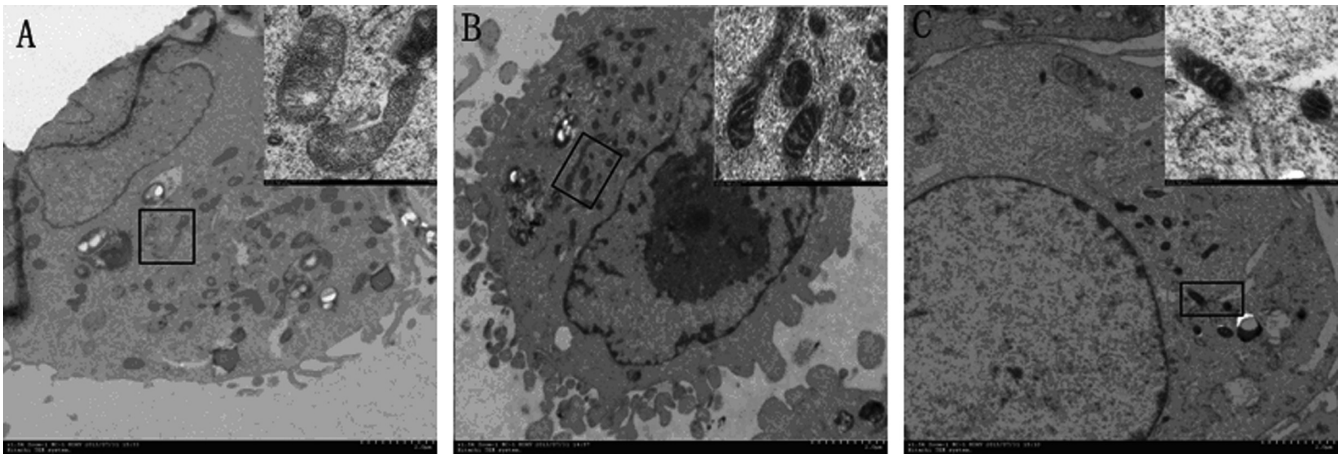

Figure 10. TEM images of mitochondria in A549/DDP cells following $TPGS_{2k}$/PLGA NPs treatments for 24 h in vitro. (A) Control; (B) $TPGS_{2k}$/PLGA NPs, 0.25 mg/mL; and (C) $TPGS_{2k}$/PLGA NPs, 0.50 mg/mL.

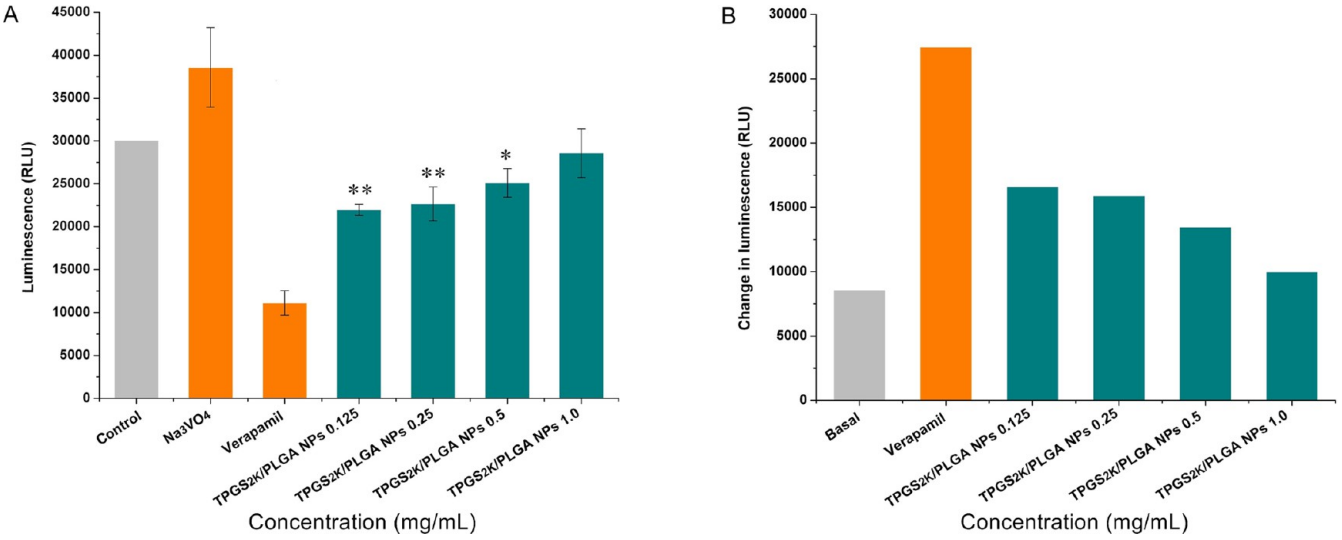

Figure 11. Effects of $TPGS_{2k}$/PLGA NPs on Pgp ATPase activity. (A) Luminescence was read under an automatic microplate reader. Negative control, Na_3VO_4 (100 μM), verapamil (200 μM), and $TPGS_{2k}$/PLGA NPs (0.125, 0.25, 0.5, and 1.0 mg/mL) treated P-gp reactions were performed. (B) The relative change rate of luminescence is calculated based on the data in graph A. The decrease in luminescence of control samples compared to samples plus Na_3VO_4 represents basal P-gp ATPase activity, and the decrease in luminescence of verapamil or $TPGS_{2k}$/PLGA NP-treated samples compared to samples plus Na_3VO_4 represents sample-stimulated P-gp ATPase activity. Data represent mean ± SD (n = 3). (*) p < 0.05 and (**) p < 0.01 versus negative control.

certain damage, and transparency was reduced owing to the increased electron density. These results suggested that NPs caused injury to the mitochondria. The morphological change was consistent with the results from MMP detection and mitochondrial respiration analysis.

ATPase Assay. The influence of $TPGS_{2k}$/PLGA NPs on ATPase activity was measured using a commercial kit with artificial human P-gp enriched membrane according to the report of Batrakova et al.[46] All the tested nanoparticle-treated samples stimulated P-gp ATPase activity on account of the effect of verapamil. However, the change in the luminescence of $TPGS_{2k}$/PLGA NPs treated samples decreased compared to the verapamil group (Figure 11A).

P-gp mediated MDR might be reversed either by decreasing their transport energy synthesis or by inhibiting P-gp ATPase activity. The present work researched the impact of $TPGS_{2k}$/PLGA NPs on P-gp ATPase activity to clarify further the mechanism for reversing MDR. Our results indicated that $TPGS_{2k}$/PLGA NPs could not influence P-gp ATPase activity by itself but could inhibit verapamil-stimulated ATPase activity and weaken P-gp mediated efflux (Figure 11B). As shown in Figure 11A, luminescent signals from $TPGS_{2k}$/PLGA NP-treated samples were stronger than verapamil treated samples, demonstrated that the group treated with $TPGS_{2k}$/PLGA NPs had the lower P-gp activity. The results illustrated a concentration-dependent inhibition of verapamil-stimulated P-gp ATPase activity with $TPGS_{2k}$/PLGA NPs, further improved that $TPGS_{2k}$/PLGA NPs reversed MDR was concerned with P-gp ATPase. Our results were consistent with reports by Collnot et al. and showed that $TPGS_{1k}$ mostly influenced the membrane fluidity of Caco-2 cells rather than directly inhibiting P-gp ATPase activity.[19,47]

In summary, these studies suggested a novel mechanism for $TPGS_{2k}$/PLGA/SN-38 NPs increasing the death of MDR cell. After the endocytosis of $TPGS_{2k}$/PLGA/SN-38 NPs, SN-38 releases from the nanoparticles in the cytoplasm of human

DOI: 10.1021/am508340m
ACS Appl. Mater. Interfaces 2015, 7, 3888−3901

alveolar adenocarcinoma cells. Then, $TPGS_{2k}$/PLGA NPs may interfere with the structure and function of mitochondria, including reducing MMP, making the incrassate of cristae, and influencing the respiratory chain of mitochondria. However, $TPGS_{2k}$/PLGA NPs did not directly inhibit the enzymatic activity of P-gp ATPase. As a result, the efflux of SN-38 related to P-gp was clearly decreased, and the amount of SN-38 entering the nucleus was dramatically increased. Finally, $TPGS_{2k}$/PLGA/SN-38 NPs enhanced apoptosis of A549/DDP cells resulting from overcoming MDR (Figure 1C).

CONCLUSION

We successfully synthesized $TPGS_{2k}$ and prepared $TPGS_{2k}$/PLGA/SN-38 NPs. $TPGS_{2k}$/PLGA/SN-38 NPs had excellent physicochemical characteristics, such as global particles owing smooth surface, suitable diameter of about 100 nm, and narrow size distribution. The nanoparticles had with higher encapsulation efficiency and favorable drug released characteristic. $TPGS_{2k}$/PLGA/SN-38 NPs can lead to significantly higher cytotoxicity on MDR cells compared with free SN-38. Further studies on the mechanism for the nanoparticles in increasing the death of MDR cells showed that $TPGS_{2k}$/PLGA NPs might interfere with the microenvironment of P-gp efflux pump, particularly the structure and function of mitochondria. Therefore, $TPGS_{2k}$/PLGA NPs can reduce the generation of ATP and the release of energy for the requisite of P-gp efflux pump. The present study partly explicated the novel mechanism of $TPGS_{2k}$/PLGA NPs overcoming MDR. The results indicated that $TPGS_{2k}$-emulsified PLGA NPs could become the functional NPMs to have the ability to overcome P-gp mediated MDR and improve anticancer effect of some chemotherapy drugs as P-gp substrates.

AUTHOR INFORMATION

Corresponding Authors

*Tel./Fax: 0086-25-8589 1265. E-mail: yushuqin@njnu.edu.cn.
*Tel./Fax: +86 25 8327 2563. E-mail: q_xu68@163.com.

Author Contributions

Dong-Fang Wang and Wen-Ting Rong contributed equally to this work.

Funding

This work received financial support from NFSC (No. 81172721) of the People's Republic of China, NSFC for Talents Training in Basic Science (No. J1103507, J1210025), Suzhou Social Development Projects (No. SS201124), Suzhou Nanoresearch Special Plan (No. ZXG2013026), and Project Funded by the Priority Academic Program Development of Jiangsu Higher Education Institutions.

Notes

The authors declare no competing financial interest.

REFERENCES

(1) Correia, A. L.; Bissell, M. J. The Tumor Microenvironment is a Dominant Force in Multidrug Resistance. *Drug Resist. Updates* **2012**, *15* (1−2), 39−49.

(2) Song, X. R.; Cai, Z.; Zheng, Y.; He, G.; Cui, F. Y.; Gong, D. Q.; Hou, S. X.; Xiong, S. J.; Lei, X. J.; Wei, Y. Q. Reversion of Multidrug Resistance by Co-Encapsulation of Vincristine and Verapamil in PLGA Nanoparticles. *Eur. J. Pharm. Sci.* **2009**, *37* (3−4), 300−305.

(3) Wu, J.; Lu, Y.; Lee, A.; Pan, X.; Yang, X.; Zhao, X.; Lee, R. J. Reversal of Multidrug Resistance by Transferrin-Conjugated Liposomes Co-Encapsulating Doxorubicin and Verapamil. *J. Pharm. Pharm. Sci.* **2007**, *10* (3), 350−357.

(4) Choi, S. U.; Lee, C. O.; Kim, K. H.; Choi, E. J.; Park, S. H.; Shin, H. S.; Yoo, S. E.; Jung, N. P.; Lee, B. H. Reversal of Multidrug Resistance by Novel Verapamil Analogs in Cancer Cells. *Anticancer Drugs* **1998**, *9* (2), 157−165.

(5) Bansal, T.; Mishra, G.; Jaggi, M.; Khar, R. K.; Talegaonkar, S. Effect of P-glycoprotein Inhibitor, Verapamil, on Oral Bioavailability and Pharmacokinetics of Irinotecan in Rats. *Eur. J. Pharm. Sci.* **2009**, *36* (4−5), 580−590.

(6) Ren, T.; Wu, W.; Jia, M.; Dong, H.; Li, Y.; Ou, Z. Reduction-Cleavable Polymeric Vesicles with Efficient Glutathione-Mediated Drug Release Behavior for Reversing Drug Resistance. *ACS Appl. Mater. Interfaces* **2013**, *5* (21), 10721−10730.

(7) Ren, Y.; Wang, R.; Liu, Y.; Guo, H.; Zhou, X.; Yuan, X.; Liu, C.; Tian, J.; Yin, H.; Wang, Y.; Zhang, N. A Hematoporphyrin-Based Delivery System for Drug Resistance Reversal and Tumor Ablation. *Biomaterials* **2014**, *35* (8), 2462−2470.

(8) Zhang, Z.; Ali, M. M.; Eckert, M. A.; Kang, D. K.; Chen, Y. Y.; Sender, L. S.; Fruman, D. A.; Zhao, W. A Polyvalent Aptamer System for Targeted Drug Delivery. *Biomaterials* **2013**, *34* (37), 9728−9735.

(9) Yu, S.; Ding, J.; He, C.; Cao, Y.; Xu, W.; Chen, X. Disulfide Cross-Linked Polyurethane Micelles as a Reduction-Triggered Drug Delivery System for Cancer Therapy. *Adv. Health Mater.* **2014**, *3* (5), 752−760.

(10) Muthu, M. S.; Kulkarni, S. A.; Raju, A.; Feng, S.-S. Theranostic Liposomes of TPGS Coating for Targeted Co-Delivery of Docetaxel and Quantum Dots. *Biomaterials* **2012**, *33* (12), 3494−3501.

(11) Xie, X.; Tao, Q.; Zou, Y.; Zhang, F.; Guo, M.; Wang, Y.; Wang, H.; Zhou, Q.; Yu, S. PLGA Nanoparticles Improve The Oral Bioavailability of Curcumin in Rats: Characterizations and Mechanisms. *J. Agric. Food Chem.* **2011**, *59* (17), 9280−9289.

(12) Mu, L.; Feng, S. S. Vitamin E TPGS Used as Emulsifier in The Solvent Evaporation/Extraction Technique for Fabrication of Polymeric Nanospheres for Controlled Release of Paclitaxel (Taxol). *J. Controlled Release* **2002**, *80* (1−3), 129−144.

(13) Liu, Y.; Feng, S.-S. Surfactant Chain Length Effects on Nanoparticles of Biodegradable Polymers for Targeted Drug Delivery. *AIChE J.* **2012**, *58* (11), 3289−3297.

(14) Mi, Y.; Liu, Y.; Feng, S.-S. Formulation of Docetaxel by Folic Acid-Conjugated D-α-Tocopheryl Polyethylene Glycol Succinate 2000 (Vitamin E $TPGS_{2k}$) Micelles for Targeted and Synergistic Chemotherapy. *Biomaterials* **2011**, *32* (16), 4058−4066.

(15) Zhang, Z.; Tan, S.; Feng, S. S. Vitamin E TPGS as a Molecular Biomaterial for Drug Delivery. *Biomaterials* **2012**, *33* (19), 4889−4906.

(16) Wang, Y.; Guo, M.; Lu, Y.; Ding, L. Y.; Ron, W. T.; Liu, Y. Q.; Song, F. F.; Yu, S. Q. Alpha-Tocopheryl Polyethylene Glycol Succinate-Emulsified Poly(lactic-co-glycolic acid) Nanoparticles for Reversal of Multidrug Resistance in Vitro. *Nanotechnology* **2012**, *23* (49), 495103.

(17) Bernkop-Schnürch, A.; Grabovac, V. Polymeric Efflux Pump Inhibitors in Oral Drug Delivery. *Am. J. Drug Delivery* **2006**, *4* (4), 263−272.

(18) Batrakova, E. V.; Li, S.; Vinogradov, S. V.; Alakhov, V. Y.; Miller, D. W.; Kabanov, A. V. Mechanism of Pluronic Effect on P-Glycoprotein Efflux System in Blood-Brain Barrier: Contributions of Energy Depletion and Membrane Fluidization. *J. Pharmacol. Exp. Ther.* **2001**, *299* (2), 483−493.

(19) Collnot, E. M.; Baldes, C.; Schaefer, U. F.; Edgar, K. J.; Wempe, M. F.; Lehr, C. M. Vitamin E TPGS P-Glycoprotein Inhibition Mechanism: Influence on Conformational Flexibility, Intracellular ATP Levels, and Role of Time and Site of Access. *Mol. Pharmaceutics* **2010**, *7* (3), 642−651.

(20) Zhang, Z.; Liu, Z.; Ma, L.; Jiang, S.; Wang, Y.; Yu, H.; Yin, Q.; Cui, J.; Li, Y. Reversal of Multidrug Resistance by Mitochondrial Targeted Self-Assembled Nanocarrier Based on Stearylamine. *Mol. Pharmaceutics* **2013**, *10* (6), 2426−2434.

(21) Kamiyama, H.; Takano, S.; Tsuboi, K.; Matsumura, A. Anti-Angiogenic Effects of SN-38 (Active Metabolite of Irinotecan): Inhibition of Hypoxia-Inducible Factor 1 Alpha (HIF-1Alpha)/

DOI: 10.1021/am508340m
ACS Appl. Mater. Interfaces 2015, 7, 3888−3901

Vascular Endothelial Growth Factor (VEGF) Expression of Glioma and Growth of Endothelial Cells. *J. Cancer Res. Clin. Oncol.* **2005**, *131* (4), 205−213.
(22) Xu, Y.; Villalona-Calero, M. A. Irinotecan: Mechanisms of Tumor Resistance and Novel Strategies for Modulating Its Activity. *Ann. Oncol.* **2002**, *13* (12), 1841−1851.
(23) Chen, Z. S.; Furukawa, T.; Sumizawa, T.; Ono, K.; Ueda, K.; Seto, K.; Akiyama, S. I. ATP-Dependent Efflux of CPT-11 and SN-38 by the Multidrug Resistance Protein (MRP) and Its Inhibition by PAK-104P. *Mol. Pharmacol.* **1999**, *55* (5), 921−928.
(24) Papadopulos, F.; Spinelli, M.; Valente, S.; Foroni, L.; Orrico, C.; Alviano, F.; Pasquinelli, G. Common Tasks in Microscopic and Ultrastructural Image Analysis Using ImageJ. *Ultrastruct. Pathol.* **2007**, *31* (6), 401−407.
(25) Cossarizza, A.; Baccaranicontri, M.; Kalashnikova, G.; Franceschi, C. A New Method for the Cytofluorometric Analysis of Mitochondrial Membrane Potential Using the J-Aggregate Forming Lipophilic Cation 5,5′,6,6′-Tetrachloro-1,1′,3,3′-Tetraethylbenzimidazolcarbocyanine Iodide (JC-1). *Biochem. Biophys. Res. Commun.* **1993**, *197* (1), 40−45.
(26) Lu, Y.; Wang, Y. Y.; Yang, N.; Zhang, D.; Zhang, F. Y.; Gao, H. T.; Rong, W. T.; Yu, S. Q.; Xu, Q. Food Emulsifier Polysorbate 80 Increases Intestinal Absorption of Di-(2-ethylhexyl) Phthalate in Rats. *Toxicol. Sci.* **2014**, *139* (2), 317−327.
(27) Cheng, G.; Zielonka, J.; Dranka, B. P.; McAllister, D.; Mackinnon, A. C., Jr.; Joseph, J.; Kalyanaraman, B. Mitochondria-Targeted Drugs Synergize with 2-Deoxyglucose to Trigger Breast Cancer Cell Death. *Cancer Res.* **2012**, *72* (10), 2634−44.
(28) Yu, L.; Wu, W. K.; Li, Z. J.; Liu, Q. C.; Li, H. T.; Wu, Y. C.; Cho, C. H. Enhancement of Doxorubicin Cytotoxicity on Human Esophageal Squamous Cell Carcinoma Cells by Indomethacin and 4-[5-(4-Chlorophenyl)-3-(Trifluoromethyl)-1H-Pyrazol-1-yl]-Benzenesulfonamide (SC236) via Inhibiting P-Glycoprotein Activity. *Mol. Pharmacol.* **2009**, *75* (6), 1364−1373.
(29) Huang, Z.; Tong, Y.; Wang, J.; Huang, Y. NMR Studies of the Relationship Between the Changes of Membrane Lipids and the Cisplatin-Resistance of A549/DDP cells. *Cancer Cell Int.* **2003**, *3* (1), 5.
(30) Zhang, J.; Zhang, T.; Ti, X.; Shi, J.; Wu, C.; Ren, X.; Yin, H. Curcumin Promotes Apoptosis in A549/DDP Multidrug-Resistant Human Lung Adenocarcinoma Cells Through an MiRNA Signaling Pathway. *Biochem. Biophys. Res. Commun.* **2010**, *399* (1), 1−6.
(31) Xu, L.; Li, H.; Wang, Y.; Dong, F.; Wang, H.; Zhang, S. Enhanced Activity of Doxorubicin in Drug Resistant A549 Tumor Cells by Encapsulation of P-Glycoprotein Inhibitor in PLGA-Based Nanovectors. *Oncol. Lett.* **2014**, *7* (2), 387−392.
(32) Vivek, R.; Thangam, R.; NipunBabu, V.; Rejeeth, C.; Sivasubramanian, S.; Gunasekaran, P.; Muthuchelian, K.; Kannan, S. Multifunctional HER2-Antibody Conjugated Polymeric Nanocarrier-Based Drug Delivery System for Multi-Drug-Resistant Breast Cancer Therapy. *ACS Appl. Mater. Interfaces* **2014**, *6* (9), 6469−6480.
(33) Xia, H.; Gao, X.; Gu, G.; Liu, Z.; Zeng, N.; Hu, Q.; Song, Q.; Yao, L.; Pang, Z.; Jiang, X.; Chen, J.; Chen, H. Low Molecular Weight Protamine-Functionalized Nanoparticles for Drug Delivery to the Brain After Intranasal Administration. *Biomaterials* **2011**, *32* (36), 9888−9898.
(34) Zastre, J.; Jackson, J.; Bajwa, M.; Liggins, R.; Iqbal, F.; Burt, H. Enhanced Cellular Accumulation of a P-Glycoprotein Substrate, Rhodamine-123, by Caco-2 Cells Using Low Molecular Weight Methoxypolyethylene Glycol-Block-Polycaprolactone Diblock Copolymers. *Eur. J. Pharm. Biopharm.* **2002**, *54* (3), 299−309.
(35) Akazawa, Y.; Kawaguchi, H.; Funahashi, M.; Watanabe, Y.; Yamaoka, K.; Hashida, M.; Takakura, Y. Effect of Interferons on P-Glycoprotein-Mediated Rhodamine-123 Efflux in Cultured Rat Hepatocytes. *J. Pharm. Sci.* **2002**, *91* (10), 2110−2115.
(36) Barakat, S.; Gayet, L.; Dayan, G.; Labialle, S.; Lazar, A.; Oleinikov, V.; Coleman, A. W.; Baggetto, L. G. Multidrug-Resistant Cancer Cells Contain Two Populations of P-Glycoprotein with Differently Stimulated P-gp ATPase Activities: Evidence From Atomic Force Microscopy and Biochemical Analysis. *Biochem. J.* **2005**, *388* (Pt 2), 563−571.
(37) Berridge, M. V.; Herst, P. M.; Lawen, A. Targeting Mitochondrial Permeability in Cancer Drug Development. *Mol. Nutr. Food Res.* **2009**, *53* (1), 76−86.
(38) Dong, X.; Mattingly, C. A.; Tseng, M. T.; Cho, M. J.; Liu, Y.; Adams, V. R.; Mumper, R. J. Doxorubicin and Paclitaxel-Loaded Lipid-Based Nanoparticles Overcome Multidrug Resistance by Inhibiting P-Glycoprotein and Depleting ATP. *Cancer Res.* **2009**, *69* (9), 3918−3926.
(39) Abe, Y.; Sakairi, T.; Kajiyama, H.; Shrivastav, S.; Beeson, C.; Kopp, J. B. Bioenergetic Characterization of Mouse Podocytes. *Am. J. Physiol. Cell Physiol.* **2010**, *299* (2), C464−476.
(40) Zhang, J.; Nuebel, E.; Wisidagama, D. R.; Setoguchi, K.; Hong, J. S.; Van Horn, C. M.; Imam, S. S.; Vergnes, L.; Malone, C. S.; Koehler, C. M.; Teitell, M. A. Measuring Energy Metabolism in Cultured Cells, Including Human Pluripotent Stem Cells and Differentiated Cells. *Nature Protocols* **2012**, *7* (6), 1068−85.
(41) Zhou, H.; Zhang, B.; Zheng, J.; Yu, M.; Zhou, T.; Zhao, K.; Jia, Y.; Gao, X.; Chen, C.; Wei, T. The Inhibition of Migration and Invasion of Cancer Cells by Graphene via the Impairment of Mitochondrial Respiration. *Biomaterials* **2014**, *35* (5), 1597−1607.
(42) Toogood, P. L. Mitochondrial Drugs. *Curr. Opin. Chem. Biol.* **2008**, *12* (4), 457−63.
(43) Neuzil, J.; Dyason, J.; Freeman, R.; Dong, L.-F.; Prochazka, L.; Wang, X.-F.; Scheffler, I.; Ralph, S. Mitocans as Anti-Cancer Agents Targeting Mitochondria: Lessons From Studies with Vitamin E Analogues, Inhibitors of Complex II. *J. Bioenerg. Biomembr.* **2007**, *39* (1), 65−72.
(44) Zhao, Y.; Neuzil, J.; Wu, K. Vitamin E Analogues as Mitochondria-Targeting Compounds: From the Bench to the Bedside? *Mol. Nutr. Food Res.* **2009**, *53* (1), 129−139.
(45) Dong, L. F.; Low, P.; Dyason, J. C.; Wang, X. F.; Prochazka, L.; Witting, P. K.; Freeman, R.; Swettenham, E.; Valis, K.; Liu, J.; Zobalova, R.; Turanek, J.; Spitz, D. R.; Domann, F. E.; Scheffler, I. E.; Ralph, S. J.; Neuzil, J. Alpha-Tocopheryl Succinate Induces Apoptosis by Targeting Ubiquinone-Binding Sites in Mitochondrial Respiratory Complex II. *Oncogene* **2008**, *27* (31), 4324−35.
(46) Batrakova, E. V.; Li, S.; Alakhov, V. Y.; Miller, D. W.; Kabanov, A. V. Optimal Structure Requirements for Pluronic Block Copolymers in Modifying P-Glycoprotein Drug Efflux Transporter Activity in Bovine Brain Microvessel Endothelial Cells. *J. Pharmacol. Exp. Ther.* **2003**, *304* (2), 845−54.
(47) Collnot, E. M.; Baldes, C.; Wempe, M. F.; Kappl, R.; Huttermann, J.; Hyatt, J. A.; Edgar, K. J.; Schaefer, U. F.; Lehr, C. M. Mechanism of Inhibition of P-Glycoprotein Mediated Efflux by Vitamin E TPGS: Influence on ATPase Activity and Membrane Fluidity. *Mol. Pharmaceutics* **2007**, *4* (3), 465−74.

DOI: 10.1021/am508340m
ACS Appl. Mater. Interfaces 2015, 7, 3888−3901